Methodology for brick/mortar interface strength characterization at high temperature

Jérôme Brulin, Eric Blond, Emmanuel de Bilbao, Amna Rekik, Alain Gasser, Matthieu Landreau, Yannick Colleville

Methodology for brick/mortar interface strength characterization at high temperature

Jérôme Brulin[1], Eric Blond[2], Emmanuel de Bilbao[3], Amna Rekik[2], Matthieu Landreau[4], Alain Gasser[2], Yannick Colleville[2]

[1] *Saint-Gobain Research Provence, 550 avenue A. Jauffret, 84306 Cavaillon, France*
[2] *Univ. Orléans, Univ. Tours, INSA-CVL, LaMé, 8 rue L. de Vinci, 45072 Orléans, France*
[3] *CEMHTI (CNRS, UPR3079), 1D avenue de la Recherche Scientifique, 45072 Orléans, France*
[4] *ArcelorMittal France, 3031 rue du Comte Jean, CS 52508, 59381 Dunkerque Cedex 1, France*

jerome.brulin@saint-gobain.com, eric.blond@univ-orleans.fr, emmanuel.debilbao@univ-orleans.fr, amna.rekik@univ-orleans.fr, matthieu.landreau@arcelormittal.com, alain.gasser@univ-orleans.fr, yannick.colleville@univ-orleans.fr

Abstract:
The interface between bricks and mortar is often the weakest part of masonry structures. For refractory linings, the interface strength must be measured at high temperature. Adapted slant shear tests and a new dedicated tensile test set up are proposed here for this purpose. To test the ability of the proposed method, it was applied on two representative brick/mortar couples from room temperature up to 1450°C. Slant shear tests were conducted to measure ultimate compression and shear stresses and to identify temperature dependent parameters of the Mohr-Coulomb failure criterion. Tensile tests were performed to identify the tensile cut-off. Depending on the brick/mortar couples, the failure can appear at the interface or in the mortar. Cohesion and tensile strength decrease sharply over 900°C.

Keywords: refractory materials, high temperature, tensile test, slant shear test, brick/mortar interface strength, Mohr-Coulomb criterion.

1. Introduction

High temperature industries (i.e. steel or gas industries, glass making, …) require structures made of many different linings, from inside to outside: a working lining in contact with hot products, a safety lining, an insulating lining, and an outer steel shell. Parts of these linings consist of refractory masonries, with or without mortar. Masonry structure modelling is studied extensively owing to its wide application in many other fields such as civil engineering or cultural heritage renovation [1-3 for example].
Quasi-brittle materials, such as concrete, mortar, ceramics or refractory materials, generally fail due to progressive crack growth. This mechanical behaviour is usually explained by the heterogeneity of the material due to the presence of different phases and material flaws. The modelling of the thermo-mechanical behaviour of refractory materials presents many difficulties in common with concrete and geo-materials (e.g. asymmetric damage behaviour, interaction with the environment) added to particular effects due to service temperature in the range 800°C – 1600°C such as the appearance of asymmetric creep behaviour [4]. However, in the case of masonries, cracks appear most of the time at the brick/mortar interface because it is generally the weakest link of the assembly [5]. This observation, associated with the quasi-

brittle behaviour of mortar, leads to the definition of a discrete damage kinetic law for masonry. This assumption is at the origin of the development of a homogeneous equivalent material with behaviour depending on the "joint state" [6], i.e. perfect interface or broken joint. This approach was first used in the particular case of mortarless refractory masonries, to model the bottom working lining of a steel ladle with an adapted joint state definition: open or closed [7]. In view of the promising results obtained, the approach was refined and experimentally validated at room temperature by Nguyen *et al.* [8], confirming the ability of a model based on the homogenisation of the masonry combined with a "joint state concept" to reproduce the whole behaviour of a wall. An extension of this joint state concept, initially developed for 2D masonries at room temperature, to 3D refractory masonries with temperature dependent behaviour was then proposed by Landreau *et al.* [9].

In refractory applications, the high thermal gradient across the wall induces tensile stresses on the cold face. Moreover, the thermal expansion is never totally free in the whole structure and it can locally induce bending of the refractory lining, and thus tensile stresses in one part of the structure. As a result, refractory brick/mortar interfaces can fail under tensile load and under compression - shear load. It is therefore necessary to characterize the refractory brick/mortar interface with respect to these solicitations from room temperature up to 1500°C. The combined compression/shear load in masonries is widely investigated in civil engineering with the classical shear wall test [10] and deep-beam test [1]. At a local scale, dedicated devices have been developed to test brick/mortar interfaces. Figure 1 shows the main principles used to apply normal and tangential controlled stresses. Tests on two bricks pasted by one mortar joint as on the top right of Figure 1 [11, 12] or on three bricks pasted by two mortar joints as on the bottom left [13, 14] are the most frequently used. It is worth mentioning that the European standard corresponds to the test presented on the bottom left of Figure 1 [15]. Some authors have proposed more complicated tests on larger structures to ensure stress homogeneity [16]. However, to the best of our knowledge, in every case available in the literature, these tests were performed at room temperature.

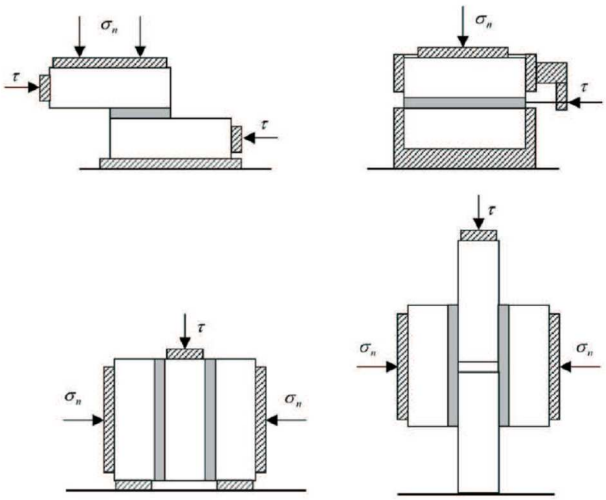

Figure 1: Set of devices for shear tests [11]

On the other hand, although tensile fracture has also been considered in civil engineering [17-19], it has been less studied in the framework of brick/mortar interfaces [20]. Tensile fracture is increasingly studied in refractory materials with crack propagation tests such as the wedge splitting test for example [21]. The bending test is the most popular mechanical test at high temperature since it is the easiest to perform in the range 800°C – 1600°C even if it is difficult to use the experimental data properly [22, 23]. However, this test is not fully suitable to study

brick/mortar interface strength because the stress field is not homogeneous in the section of the sample, as is also the case in the wedge splitting test [21].

Different test methods can be used to apply a tensile stress through a section of a specimen. Devices and set-ups have been developed to perform tensile tests on monolithic refractory samples at high temperature [24, 25]. They require sample preparation to ensure clamping and alignment which might damage the samples (made of an assembly of bricks and joints). On the other hand, Almeida *et al.* [26] presented a brief summary of methods to characterize the tensile strength of joints based on direct tensile tests, crossed brick couplets and bending tests. The direct tensile test is the best method to study the tensile behaviour but some technical problems were pointed out by van Mier and van Vliet [27] such as the alignment of the loading chain including the specimen, the preparation of the specimen itself and the gripping. Different specially designed clamping devices have therefore been developed to be used at room temperature but all of them are too bulky to be placed in a furnace. Moreover, the materials used cannot withstand high temperature. Crossed brick couplets and bending devices present the same problem.

Other experimental set-ups exist in the refractory community, but they were designed to identify complex tensile behaviour relationships taking into account damage [28] or creep [24] at high temperature and do not seem to be well adapted to characterize the brick/mortar interface strength.

Finally, whatever the fracture mode investigated, to the authors' knowledge, there is not any complete set of devices to characterize the high temperature strength of interfaces. Thus, the purpose of this paper is to present two specially designed devices to identify the brick/mortar interface strength at high temperature: a slant shear test and a dedicated tensile test.

A simple model of the interface behaviour is proposed, namely an interface failure criterion based on a Mohr-Coulomb yield function (for compression and shear) and a tensile cut-off. Its parameters can be determined using the previously developed tests.

To illustrate the ability of the devices developed, two couples of bricks and mortars were considered, covering a large temperature range. The use of the experimental results to identify the interface failure criterion is also described.

2. Interface failure criterion

The shear strength of the brick/mortar interface typically depends on the normal stress applied to the interface. This friction type behaviour is classically described by the Mohr-Coulomb yield function:

$$f(\tau, \sigma_n, \Phi) = |\tau| - c + \sigma_n tan\Phi \qquad (1)$$

where τ is the shear stress, σ_n is the normal stress (negative in compression), c is the cohesion of the material and ϕ the internal angle of friction (Figure 2). Determining cohesion and the internal friction angle requires the measurement of normal and shear stresses until failure.

A tensile cut-off corresponding to tensile failure is added in order to complete the interface failure criterion. It is defined by:

$$f(\sigma_n, f_t) = \sigma_n - f_t \qquad (2)$$

where f_t is the tensile strength (Figure 2). In a tensile test of a quasi-brittle material, carried out under controlled displacement, the tensile strength corresponds to the peak of the stress-displacement curve.

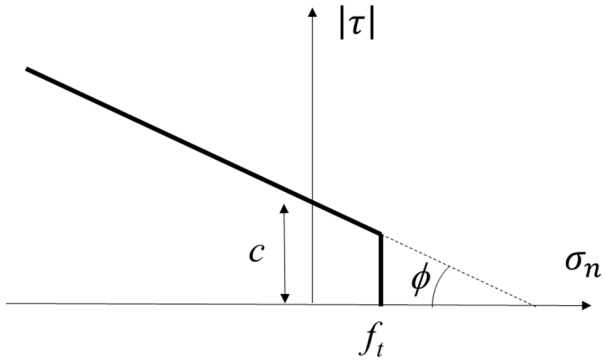

Figure 2: Failure surface (shear stress versus normal stress) of brick/mortar interface.

It can be noted that this criterion concerns the interface failure, but it can also include the failure of the mortar. So it can model globally the failure of the joint (brick/mortar interface and mortar).

3. Materials

Depending on the brick and mortar compositions, various kinds of bonds can take place between mortar and brick. An interface is defined by the couple of brick and mortar. In this work, the two couples considered are typically dedicated to high temperature industries. The first one was made of dense silica bricks with a silica based mortar (used in coke ovens), denoted A. The second was made of high alumina bricks with a high alumina mortar, denoted B, which is used in blast furnaces. Information on the composition of the bricks and mortars is summarized in Table 1.

w. %	A		B	
	Brick	Mortar	Brick	Mortar
SiO_2	95	95	25	
CaO	< 3	< 1		
Al_2O_3	< 1.5	< 1	72	90
Fe_2O_3	<1	<0.5	< 1	< 1

Table 1: Composition of refractory bricks and mortars

Such refractory materials have to be stabilized before being tested. For interface A, the silica bricks were previously heated to stabilize quartz into cristobalite. For interface B, the high alumina bricks were previously stabilized into mullite mineralogical form. Then, green mortar was shaped between the two half samples, followed by hardening at room temperature during 24 hours and drying at 110°C during 24 hours.
The interface strength obviously depends on the couple of materials, but workmanship is also a crucial factor. However, the purpose of this paper is to present the experimental methods developed to characterize the interface strength at high temperature, and to show how to use them to determine the parameters of the interface failure criterion.

4. Compression - shear strength characterization

2.1 Experimental set-up

To characterize the shear strength from room temperature up to 1600°C, the loading set-up must be put in an appropriate furnace. This constraint induces two major difficulties: firstly, the set-up must be compact enough; secondly, the loading device must withstand high temperature. A possible solution to overcome these difficulties is to perform a slant shear test on two bricks pasted by one inclined mortar joint, as presented in Figure 3. This particular design of the specimen makes it possible to apply normal and shear stresses at the interface with a standard compression device. This type of test is a standard to characterize the adhesion of a repair material on concrete [29] and is also used to characterize the adhesion between two different concretes for example [30]. The limits of this test at room temperature and the influence of different shapes and material parameters were studied by Austin et al. [31]. The standard and usual test includes only one interface and is performed at room temperature while the specimen studied here includes two parallel interfaces and is performed at high temperature. The same test was used by Raffard et al. [32] coupled to optical measurement at room temperature to characterize the equivalent interface stiffness as a function of the mortar slant angle.

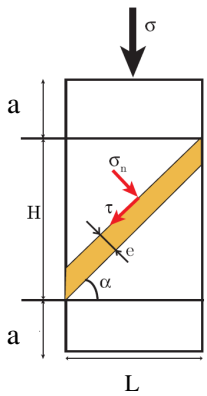

Figure 3: Slant shear test specimen.

The local normal compression σ_n and shear τ stresses applied on the brick/mortar interface are driven by the slant of the joint:

$$\begin{cases} \sigma_n = \sigma \cdot \cos^2 \alpha \\ \tau = \sigma \cdot \cos\alpha \sin\alpha \end{cases} \quad (1)$$

where σ is the global homogeneous applied compression stress and α is the angle between the mortar joint and the plane normal to the compression loading axis (Figure 3). The global homogeneous applied compression stress σ is computed by dividing the applied force F by the specimen transverse area S.

The identification of the cohesion and internal friction angle requires at least three different slant angles as three points are the minimum to obtain an objective line. The choice of the angle values is driven by mechanical constraints and experimental feasibilities. Indeed, to produce a shear fracture instead of a compression one, the angle must maximize the ratio of shear stress to normal compression stress. So, angles superior or equal to 45° are necessary (see Figure 4).

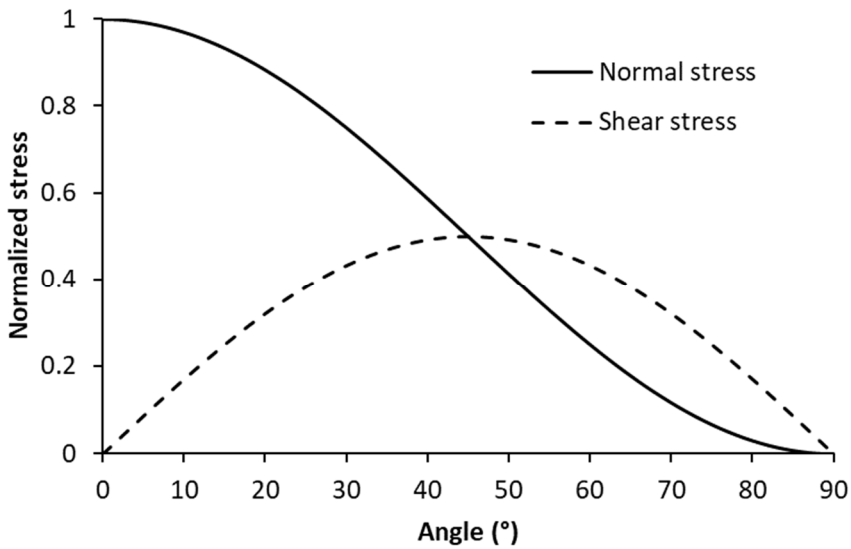

Figure 4: Evolution of shear and normal stresses at the brick/mortar interface as a function of the angle in a slant shear test.

Furthermore, the size of the specimen must be compatible with the size of the homogeneous temperature area in the furnace. This constraint is deduced from geometrical considerations and can be expressed by:

$$\begin{cases} \dfrac{e + L\sin\alpha}{\cos\alpha} + 2a \leq H_f \\ L \leq \phi_f \end{cases} \qquad (2)$$

where a is the distance between the top (or the bottom) of the specimen and the closest intersection of the mortar joint with the lateral surface of the sample (see Figure 3). L is the largest specific dimension of sample section, while e is the thickness of the mortar joint. H_f and ϕ_f are respectively the height and diameter of the cylindrical area in the furnace chamber which provides a homogeneous temperature field. Finally, the chosen specimen shape is a parallelepiped of section 35x35 mm^2 (i.e. L = 35 mm) with a = 15 mm. Its total height depends on the mortar joint angle α.

2.2 Specimen preparation and test conditions

The mortar thickness was 4 mm for samples A and 2 mm for samples B.
Samples A were first heated up to 1000°C, followed by a dwell of one hour to stabilize the mortar. Then, the samples were heated up or cooled down to the temperature of the test. A second dwell of 30 minutes at the temperature of the test was applied before performing the test to achieve the thermal treatment of the bonding. The tests were performed at 800°C, 1080°C and 1350°C for the three angles 45°, 55° and 65° of the mortar joint.
Samples B were first heated up to 450°C at a rate of 350°C/h, then up to 650°C at a rate of 125°C/h and finally to the temperature of the test at 325°C/h. A dwell of one hour was applied at the temperature of the test before performing the experiment. Tests (three for each material/temperature/angle combination) were performed at room temperature, 900°C and 1450°C for the three angles 45°, 55° and 65° of the mortar joint.
The tests were performed on a universal testing machine with a standard compression device with displacement control. The displacement speed rate was tuned to 0.5 mm/min.

As the interface strength is assessed by extracting the peak value of the load/displacement curve and the corresponding normal and shear stresses (estimated using equations (3)), the uncertainty of the calculation of the normal stress can be deduced from equation (3) and from uncertainties of stress σ assessment and angle α measurement. As σ is computed from the applied force F and the area ($L*l$), the uncertainty U_σ of σ is [33]:

$$U_\sigma = \sqrt{\left(\frac{1}{L \cdot l}\right)^2 U_F^2 + \left(\frac{F}{L^2 \cdot l}\right)^2 U_L^2 + \left(\frac{F}{L \cdot l^2}\right)^2 U_l^2} \qquad (3)$$

where L and l are the length and the width of the transverse section respectively. U_X is the uncertainty of X (F, L or l in that case). The relative uncertainty of X is:

$$^R U_X = U_X / X \qquad (4)$$

The relative uncertainty of σ is then:

$$^R U_\sigma = U_\sigma / \sigma = \sqrt{\left(^R U_F\right)^2 + \left(^R U_L\right)^2 + \left(^R U_l\right)^2} \qquad (5)$$

The relative uncertainty of normal stress is:

$$^R U_{\sigma_n} = \sqrt{\left(^R U_\sigma\right)^2 + \left(2 \tan \alpha\right)^2 U_\alpha{}^2} \qquad (6)$$

The uncertainty of the determination of the shear stress can be deduced similarly from equations (3) and from measurement uncertainties of σ and α [33]. The relative uncertainty of shear stress is:

$$^R U_\tau = \sqrt{\left(^R U_\sigma\right)^2 + \left(\tan \alpha - \frac{1}{\tan \alpha}\right)^2 U_\alpha{}^2} \qquad (7)$$

Assuming $^R U_F = 0.5$ % and $^R U_L = {}^R U_l = 1.5$ %, then $^R U_\sigma = 2.2$ %. Moreover, assuming that the total angle uncertainty is equal to ± 1° ($U_\alpha = 1°$), the relative uncertainty of the normal compression stress $^R U_{\sigma n}$ increases from 3% to 4.8% for slant angles from 45° to 65°. For the shear stress, the relative uncertainty $^R U_\tau$ increases from 2.2% to 2.8%. Finally, due to the low value of stress, this uncertainty is negligible compared to possible material scattering and workmanship effects.

2.3 Results

Figure 5 presents typical fractures after testing at high temperature. In samples A, cracks were clearly located at the interface between the mortar layer and the brick. In samples B, cracks appeared mostly in the mortar. In that case, we will consider the global joint failure (interface and mortar). In accordance with the concept of bond failure envelope [31, 34] it is proposed to use an analytical exploitation of the experimental peak load.

a) Specimens A at 1080°C

b) Specimens B at 900°C

Figure 5: Specimens after testing (slant shear tests)

Figure 6 presents typical load versus displacement curves obtained during the test for specimen A. The different curves correspond to the three different joint slants tested at the same temperature of 1350°C. The maximum load (corresponding to fracture) decreases with the slant angle increase. Figure 7 presents the effect of temperature for a constant joint angle of 55°. It appears that, after a strong decrease between 800°C and 1080°C, the maximum load is stabilized for higher temperatures. Furthermore, the curves exhibit a slight evolution of the whole behaviour of the sample from brittleness to nearly ductile. Since the silica bricks are stabilized, this is due to the mortar behaviour evolution. However, the fracture is still located at the interface and it is essentially brittle.

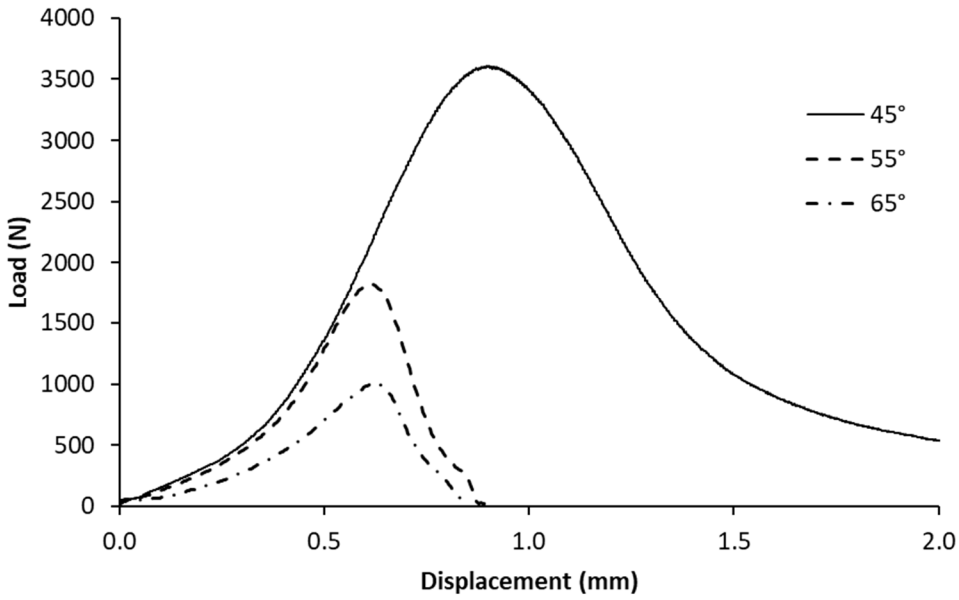

Figure 6: Load versus displacement curves for specimen A at 1350°C for three joint angles (slant shear tests)

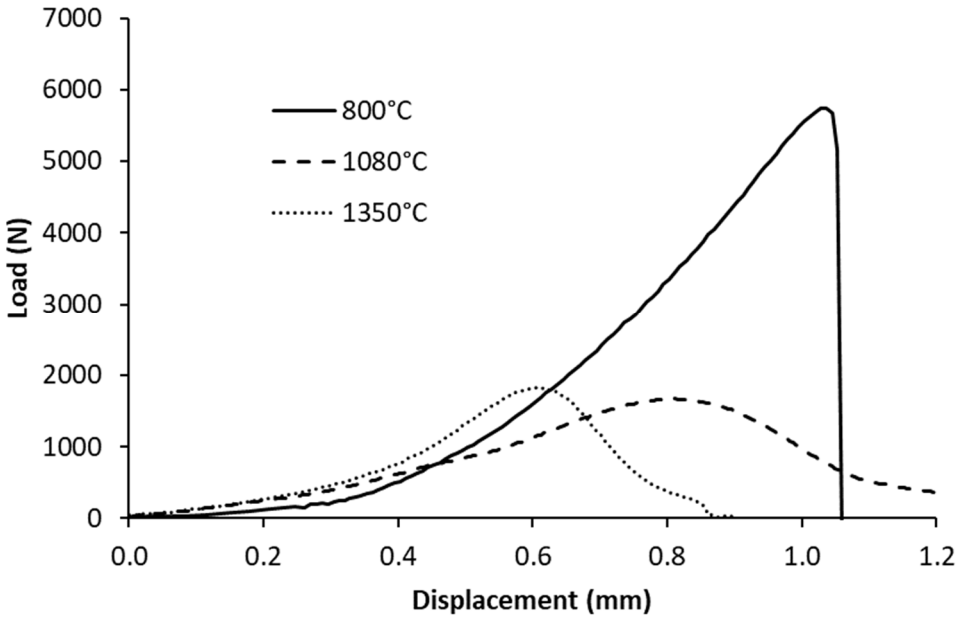

Figure 7: Load versus displacement curves for specimen A with a joint slope of 55° at different temperatures (slant shear tests)

For specimen B, typical results are presented in Figure 8. It shows (for an angle of 65°) that the maximum load of specimen B, after a slight increase until 900°C, drops drastically to almost zero. The brick/mortar interface no longer has any strength at high temperature.

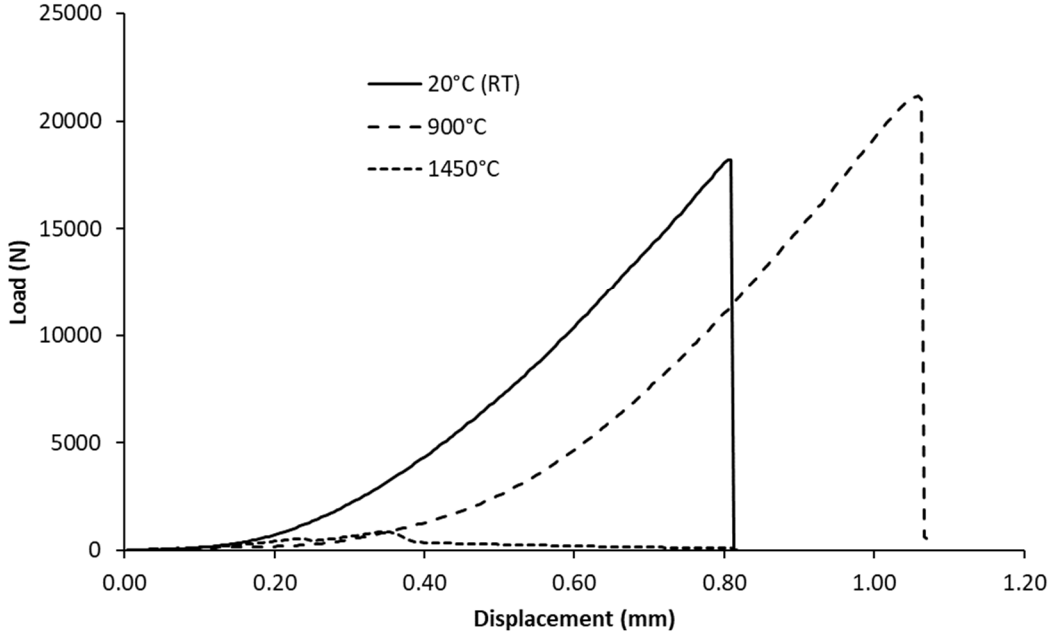

Figure 8: Load versus displacement curves for specimen B with a joint slope of 65° at different temperatures (slant shear tests)

Figure 10 shows the Mohr-Coulomb graph extracted from the load versus displacement curves of specimen A at the different temperatures tested. The ultimate strength points define a line from which the cohesion and friction angle for each temperature can be determined. The difference between 1080°C and 1350°C is small, whereas a visible difference appears for the cohesion between 800°C and 1080°C. Moreover, the friction angle does not appear to be strongly temperature dependent.

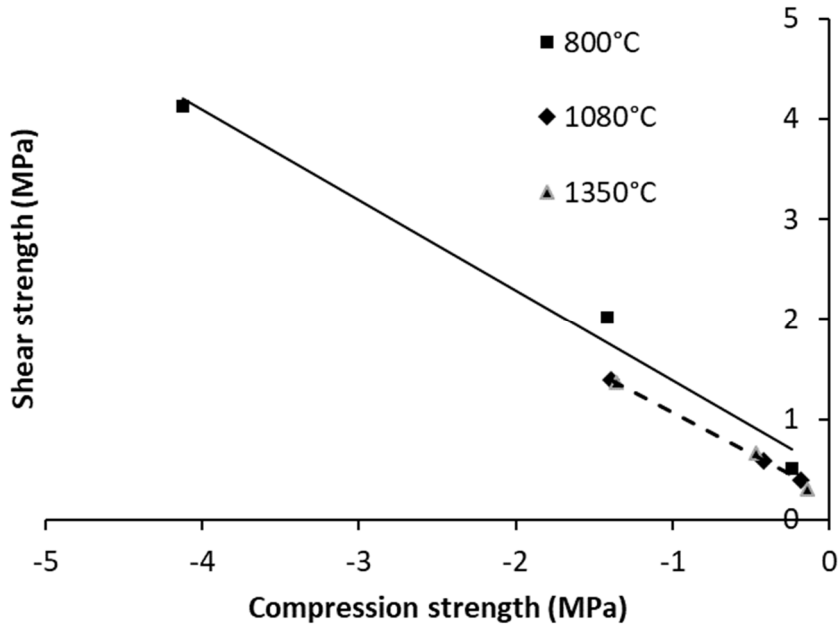

Figure 10: Mohr-Coulomb lines for specimen A at 800°C, 1080°C and 1350°C

Figure 11 presents the Mohr-Coulomb graph extracted from the load versus displacement curves on specimen B at the different temperatures tested. Firstly, there is no obvious tendency linked to the temperature. Indeed, whereas the shear strength seems to be almost independent of normal compression stress at 20°C, there is a more classical Mohr-Coulomb dependence with an enhancement of the strength value at 900°C, but a drastic drop in strength at 1450°C. This evolution is linked to the evolution of the mortar between 900°C and 1450°C. Whatever the results, this test makes it possible to quantify the shear strength evolution of the brick/mortar interface with the temperature and to identify a maximum reached at around 900°C.

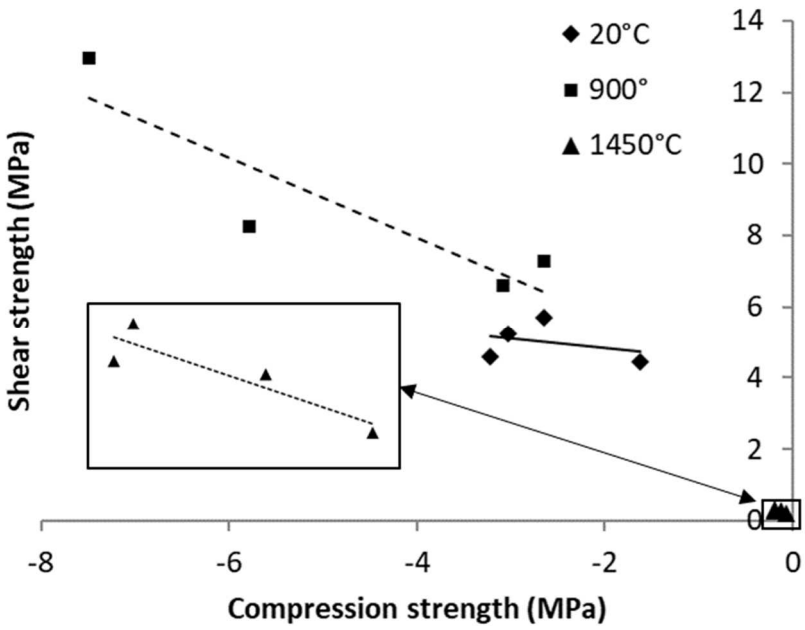

Figure 11: Mohr-Coulomb lines for specimen B at 20°C, 900°C and 1450°C

3. Tensile strength characterization

In the previous section, the Mohr-Coulomb yield surface was considered to model the mixed compression-shear strength. This section deals with the identification of the tensile cut-off corresponding to tensile failure in order to complete the interface failure criterion.

3.1 Experimental set-up

In this work, high temperature tensile strength tests were performed using a universal testing machine equipped with a high temperature furnace (Figure 13). The force was measured with a classic load cell. A cooling device is set between the furnace and the load cell to protect the load cell. The displacement of the crosshead was also measured. However, the displacement measurement does not require accuracy since only the force peak is required to determine the tensile strength.

The experimental set-up has to be compact (to be put in the furnace) and to withstand high temperatures. To ensure a pure tensile failure, it is also necessary to provide good specimen alignment. Consequently, the clamping device must withstand high temperature and its design has to ensure its installation in the confined furnace workspace (Figure 13). To that purpose,

a new set-up was designed. It consists of three parts: two clamps and an assembly including the specimen and two linking wires.

Figure 13: Universal testing machine with the furnace (AET ref. OF 25 957 Type SP)

The assembly is made up of a couple of cylindrical refractory units joined with mortar (Figure 14). Two wires, inserted in the units and going through them thanks to shouldered holes, allow the blocks to be clamped. A ball at the end of each wire stops translation. Each wire is made of nickel-chromium alloy (e.g. Nikrothal 70) to resist high temperature. It has a diameter of 2 mm so that it supports the applied stress while being flexible enough to ensure the alignment of the loading "chain". Finally, it must be long enough for the specimen to be positioned in the middle of the furnace. Both wires are gripped with specific clamps located outside the furnace, linked to cooling devices and to the testing machine. As expected, using these specific clamps and wires the specimen can be aligned in the force direction.

3.2 Specimen preparation and test conditions

It is well known that specimen dimensions and aggregate size have an influence on brittle fracture [35, 36]. Assuming that the probability of cracking increases with the joint area, it can be deduced that the smaller the sample, the higher the tensile strength for the interface. Knowing that in usual refractory linings the area of contact between bricks and mortar (2 to 4 mm thick) is around 200 × 80 mm^2, the specimens should have the same area of contact. But the specimen size is restricted by the furnace workspace as mentioned previously. The specimens were therefore chosen as large as possible, compatible with the furnace dimensions. Finally, the cylindrical units had a diameter of 20 mm, a height of 25 mm and the joint was 2 mm thick for samples B (Figure 14a). Therefore, the strength values obtained herein must be considered as an upper bound.

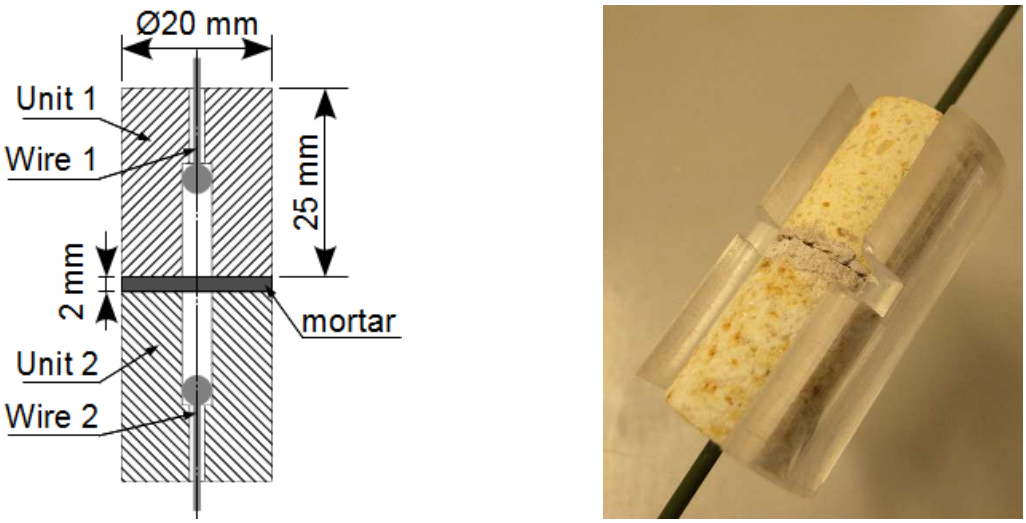

(a) (b)

Figure 14: Specially designed specimen for high temperature tensile test: principle (a), specimen and mould (b)

Ensuring a good alignment of the loading "chain" requires meticulous preparation of specimens. To that purpose, the units were obtained by core drilling. Then the core samples were ground to allow the drilling of coaxial holes. The two units were assembled using a specific mould (Figure 14b) to ensure the good alignment between the two cylinders and to control the mortar thickness. After air drying for 24 hours, the specimen was removed from the mould to be pre-heated at a temperature of 300°C.

The tensile test can be divided into 3 main stages. In the first step the specimen was put into the furnace, then tightened and clamped through the wires, heated up to the set point value at a rate of 700 °C/h and stabilised during half an hour. In the second stage, the measured force was reset to zero because the wires and load cell had expanded. The test started applying a displacement to the upper crosshead. The last stage consisted in stopping the heating device, cooling down the specimen and removing it.

Tensile tests were performed on samples A at room temperature and on samples B at three temperatures: room temperature, 900 and 1200°C. For room temperature, the tests were performed with a displacement rate of 0.5 mm/min. For high temperature tests, the displacement rate was tuned to 30 mm/min to avoid wire creep. This displacement rate has a great influence at high temperature on the Nikrothal cable behaviour and a smaller influence on the refractory behaviour up to 1200°C (the influence is higher for higher temperatures). But the interface strength was assumed to be independent of the strain rate.

The tensile strength f_t was determined using the equations:

$$f_t = \frac{F_{\max}}{S} \qquad (10)$$

$$S = \pi \frac{D^2 - d^2}{4} \qquad (11)$$

where F_{max} is the maximum load reached before the fracture of the sample, S is the area of the transverse section, D and d are the outer and the inner diameters of the cylindrical unit respectively.

The uncertainty of the determination of the tensile strength f_t can be deduced from equations (10, 11) and from the measurement uncertainties of F_{max}, D and d [33]. The relative uncertainty of tensile strength is:

$$ {}^{R}U_{f_t} = \sqrt{\underbrace{{}^{R}U_F{}^2}_{U_1^2} + \underbrace{\left(\frac{2D^2}{D^2-d^2}\right)^2 {}^{R}U_D{}^2}_{U_2^2} + \underbrace{\left(\frac{2d^2}{D^2-d^2}\right)^2 {}^{R}U_d{}^2}_{U_3^2}} \qquad (12) $$

where ${}^{R}U_F$, ${}^{R}U_D$, and ${}^{R}U_d$ are the relative uncertainties of F, D and d respectively. For the sake of simplicity, let us give a name to each of the three parts of the relative uncertainty (equation 12):

$$ U_1 = {}^{R}U_F \qquad (13) $$

$$ U_2 = \left(\frac{2D^2}{D^2-d^2}\right) {}^{R}U_D \qquad (14) $$

$$ U_3 = \left(\frac{2d^2}{D^2-d^2}\right) {}^{R}U_d \qquad (15) $$

Figure 15 represents the sensitivity of the tensile strength to the outer diameter D for an inner diameter d = 4 mm. Each part of the tensile strength uncertainty (U_1, U_2, U_3) and the combined relative uncertainty ${}^{R}U_{ft}$ (denoted U_f in Figure 15) are plotted versus the outer diameter, with ${}^{R}U_F$ = 0.5 %, ${}^{R}U_D$ = 2.5 % and ${}^{R}U_d$ = 5 %. The combined uncertainty is a quadratic fraction of D while all other parameters are constant. As a result, uncertainty decreases with an increasing diameter. For a larger diameter, the uncertainty decreases more gradually and tends to an asymptotic value equal to the square root of the quadratic sum of the relative uncertainties. The second term U_2 is larger than the others and the combined uncertainty is approximately twice as large as the relative uncertainty of the measurement of the outer diameter. As a result, the chosen diameter (20 mm) appears to be a good compromise to ensure homogeneity, compatibility with the furnace workspace and satisfactory uncertainty.

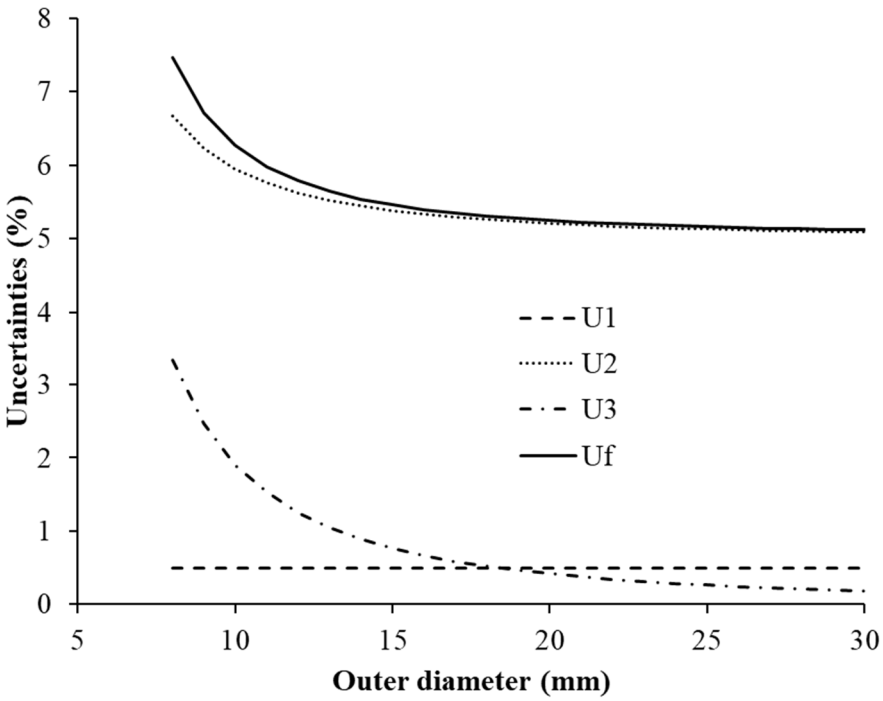

Figure 15: Uncertainties of tensile strength versus outer diameter

3.3 Results

Figure 16 presents typical load versus displacement curves obtained during the tensile test. The curves correspond to tests carried out for two specimens B at 900°C. The first nonlinear part of the curve before cracking can be explained by the nonlinear behaviour of the interface but also by the straightening out of the wires followed by their creep. Accordingly, it is difficult to deduce a behaviour model of the specimen. However, the tensile strength can be determined from the maximum load. The curve for specimen B-2 shows a load release around 4 mm of displacement. This might be due to the sliding of the wires into the bricks or to a local crushing in the area of contact between a wire ball and the specimen. Once the balls made at the end of the wires have found their places in the holes, the load increases again as if nothing had happened. It can be assumed then that this technical problem does not influence the tensile strength. After the maximum load value is reached, the load decreases very quickly for both curves because of the total failure of the joint.

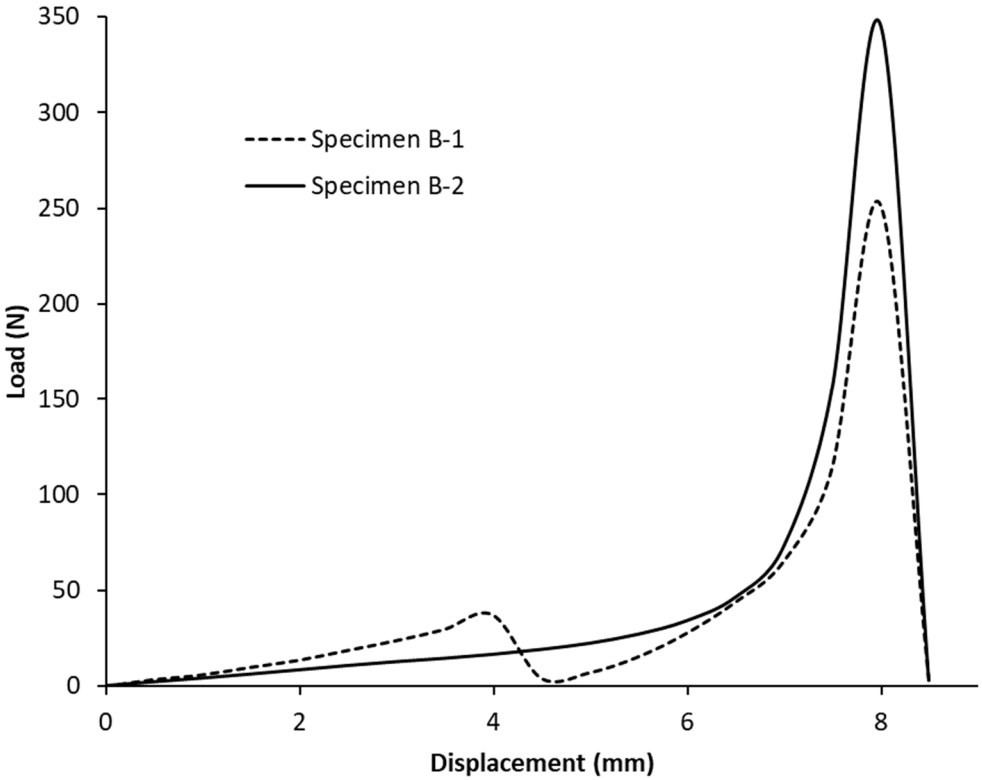

Figure 16: Load versus displacement for sample B at 900°C

The tensile strengths f_t for specimens B-1 and B-2 are 0.82 MPa (load = 247 N) and 1.1 MPa (load = 342 N) respectively.

Figure 17 presents the evolution of the tensile strength versus temperature for specimens B. The curve can be divided into two parts. The tensile strength remains nearly constant from room temperature up to 900°C. In contrast, the second portion of the curves reveals a sharp decrease. The tensile strength of specimens B is low at high temperature, which implies joint opening (brick/mortar separation) when they are submitted to a low tensile load in a structure.

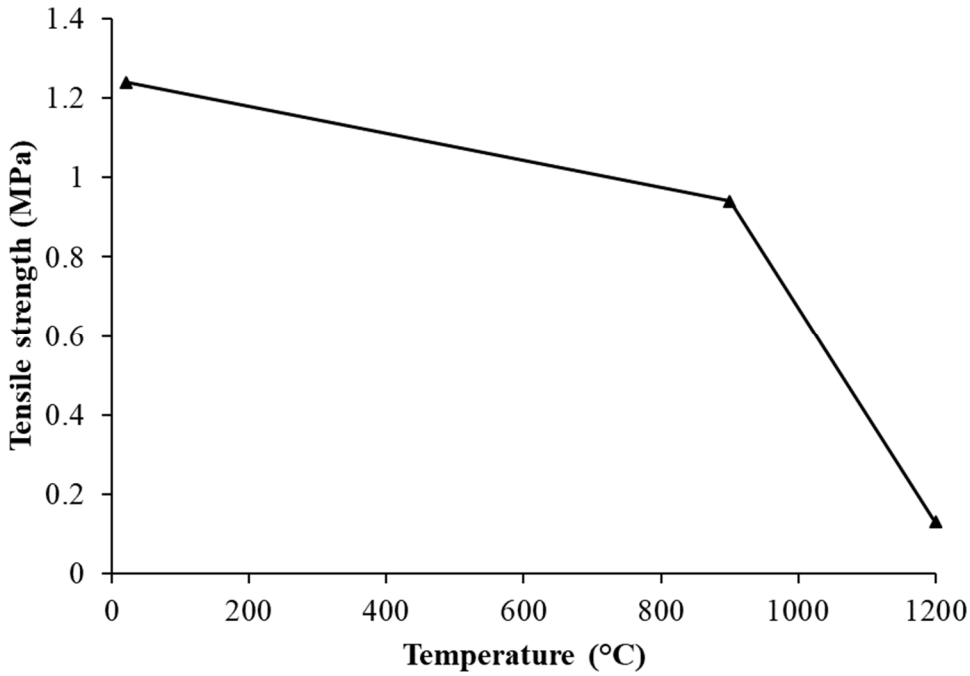

Figure 17: Tensile strength versus temperature for specimens B.

Concerning specimen A, the tensile strength at room temperature is very low (0.2 MPa). It corresponds to the failure of the brick/mortar interface (see Figure 18 with the penny shape of the mortar after failure). This shows that the bond between mortar and brick is weak. It is the reason why no tests were performed at high temperature for specimens A. The tensile strength can be considered as zero whatever the temperature for specimens A.

Figure 18: Specimen A failure in tension.

4. Failure criterion identification and discussion

Based on the tensile tests and slant shear tests performed in the previous sections, the different parameters of the Mohr-Coulomb failure criterion coupled with a tensile cut off were determined. Their values are given in Table 2. The corresponding failure surfaces are presented in Figures 19 (specimens A) and 20 (specimens B) for different temperatures.

	Specimen A			Specimen B		
Temperature	c (MPa)	tan ϕ	f_t (MPa)	c (MPa)	tan ϕ	f_t (MPa)
R.T.			0.2	4.26	0.28	1.29
800°C	0.48	0.90				
900°C				3.44	1.12	0.99
1080°C	0.24	0.82				
1350°C	0.22	0.85				
1450°C				0.15	0.81	0.14

Table 2: Cohesions, friction angles and tensile strengths identified at different temperatures

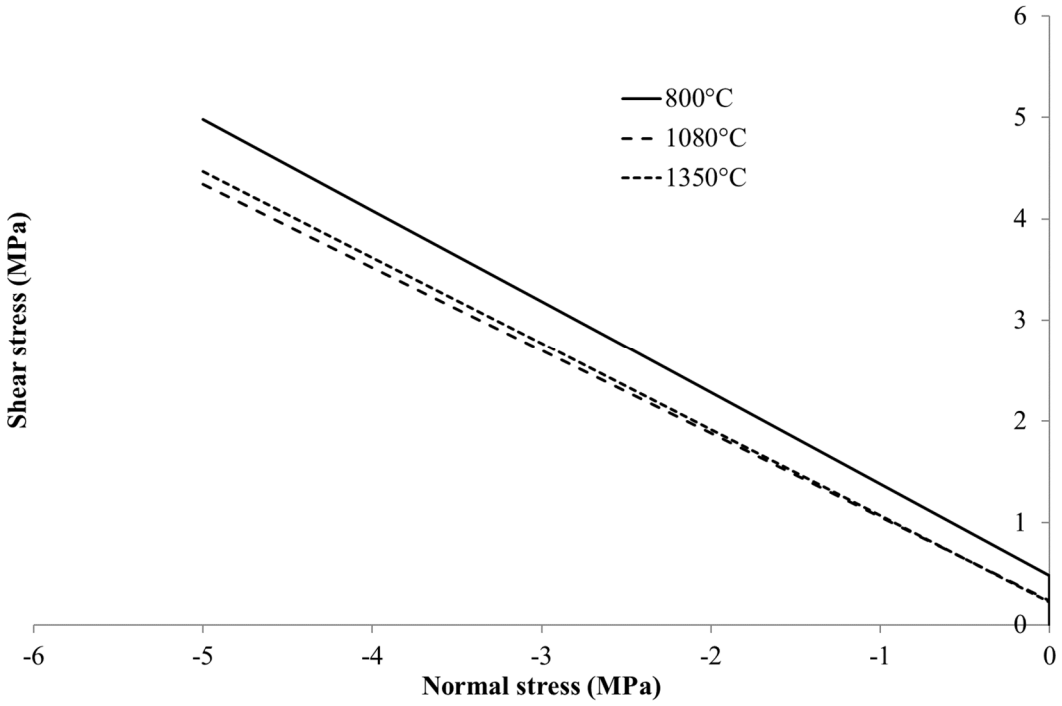

Figure 19: Failure surfaces of specimen A at different temperatures.

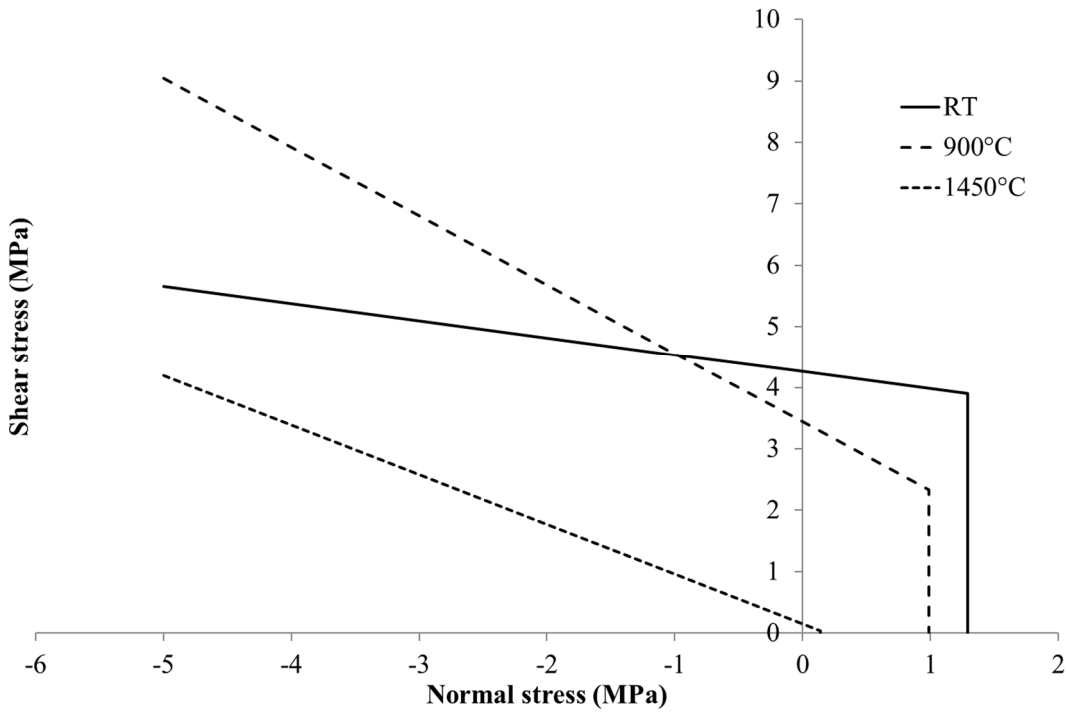

Figure 20: Failure surfaces of specimen B at different temperatures.

For specimens A, the friction angle is almost independent from temperature, while the cohesion is temperature dependent (but the values are small, near zero). The tensile strength is also small and can be considered as zero. The brick/mortar interface is very weak. No real bond is created between the two materials during heating, and a small shear or tensile load causes interface failure. Brick and mortar can be considered as two independent parts in contact with friction.

For specimens B, friction angle, cohesion and tensile strength are temperature dependent. A marked decrease in the specimen properties can be observed for temperatures higher than 900°C. In particular at 1450°C, the interface strength is weak, as for specimens A. These observations on mechanical behavior are coherent with the possible development of an increasing amount of glassy phase inside the mortar when the temperature increases. As previously pointed out, in the case of specimens B, the failure appeared mostly in the mortar: the mortar is weaker than the brick/mortar interface. So the joint property decrease at high temperatures is due to the decrease of mortar strength at these high temperatures.

5. Conclusion

Experimental characterization of the strength of the brick/mortar interface is a key point to ensure the reliability of masonry computation, as the brick/mortar interface is often the weakest link of the assembly. Although the characterization of interfaces at room temperature has been extensively studied in civil engineering, there is a real lack of data for high temperature masonry based on refractory materials.

Two set-ups and sample shapes were developed to carry out tensile and slant shear tests at high temperature. For the first one, dedicated clamping devices were designed and tests were performed in a temperature range from room temperature up to 1200°C. Results have allowed us to identify the tensile strength of the brick/mortar interface depending on the temperature. The slant shear test was carried out in the temperature range from room temperature up to

1450°C. Mohr-Coulomb parameters of the brick/mortar interface (i.e. cohesion and friction angle) were identified and found to be temperature dependent.

For both methods, the uncertainties of the strength estimation induced by the specimen geometry and measurement device were computed. Results have shown that the uncertainty is lower than 5% for tensile, compression and shear strengths. These values confirm that the discrepancy between experimental values can be explained mainly by the discrepancy between the samples (i.e. mortar batch, refractory heterogeneity).

The two different brick/mortar couples tested are representative of the two possible joint failures: brick/mortar interface or mortar. As a result, the failure surfaces obtained (Mohr-Coulomb criterion) represent the global failure of the joint and not only the failure of the brick/mortar interface.

In conclusion, the two experimental set-ups proposed here enable a complete and accurate characterization of the brick/mortar interface strength at high temperature to be carried out. The relative simplicity of these devices may facilitate their use in the refractory community to enlarge the knowledge on the ultimate strength evolution with temperature of such interfaces.

Acknowledgements

This work was supported by St-Gobain Research Provence and Centre de Pyrolyse de Marienau (CPM) companies.

References

[1] A.W. Page, Finite Element Model for Masonry. J. of Struct. Div. 104 (1978) 1267-1285.

[2] P.B. Lourenço, Computational strategies for masonry structures, PhD thesis, Delft University of Technology, The Netherlands, 1996.

[3] A. Rafiee, M. Vinches, C. Bohatier, Modelling and analysis of the Nîmes arena and the Arles aqueduct subjected to a seismic loading, using the Non-Smooth Contact Dynamics method. Eng. Struct. 30 (2008) 3457-3467.

[4] E. Blond, N. Schmitt, F. Hild, J. Poirier, P. Blumenfeld, Modelling of high temperature asymmetric creep behaviour of ceramics. J. of Eur. Ceram. Soc. 25 (2005) 1819–1827.

[5] J.L. Miranda Dias, Cracking due to shear in masonry mortar joints and around the interface between masonry walls and reinforced concrete beams. Constr. and Build. Mater. 21 (2007) 446-457.

[6] R. Luciano, E. Sacco, Homogenization technique and damage model for old masonry material. Int. J. of Solids and Struct. 34 (1997) 3191-3208.

[7] A. Gasser, K. Terny-Rebeyrotte, P. Boisse, Modelling of joint effects on refractory lining behaviour. Proc. of the Inst. of Mech. Eng., Part L: J. of Mater.: Des. and Appl. 218 (2004) 19-28.

[8] T.M.H. Nguyen, E. Blond, A. Gasser, T. Prietl, Mechanical homogenisation of masonry wall without mortar. Eur. J. of Mech. - A/Solids 28 (2009) 535-544.

[9] M. Landreau, E. Blond, A. Gasser, D. Isler, Modelling of a coke oven heating wall. UNited International TEchnical Congress on Refractory, Bahia, Brazil, 2009.

[10] T.M.J. Raijmakers, A. Vermeltfoort, Deformation controlled tests in masonry shear walls. Technical report (in Dutch) TNO-Bouw, Delft, The Netherlands, 1992.

[11] L. Abdou, R.A. Saada, F. Meftah, A. Mebarki, Experimental investigations of the joint-mortar behaviour. Mech. Res. Commun. 33 (2006) 370-384.

[12] K. Chaimoon, M.M. Attard, Modelling of unreinforced masonry walls under shear and compression. Eng. Struct. 29 (2007) 2056-2068.

[13] J.R. Riddington, P. Jukes, A masonry joint shear strength method. Proceedings of the ICE – Structures and buildings 104 (1994) 267-274.

[14] A.Gabor, A. Bennani, E. Jacquelin, F. Lebon, Modelling approaches of the in-plane shear behaviour of unreinforced and FRP strengthened masonry panels. Compos. Struct. 74 (2006) 277-288.

[15] CEN, European norm for methods of test for masonry – Part 3: Determination of initial shear strength. prEN 1052-3, 1996.

[16] P.B. Lourenço, J.O. Barros, J.T. Oliveira, Shear testing of stack bonded masonry. Constr. and Build. Mater. 18 (2004) 125-132.

[17] E.P. Prado, J.G.M. van Mier, Effect of particle structure on mode I fracture process in concrete. Eng. Fract. Mech. 70 (2003) 1793-1807.

[18] K.W. Kim, Y.S. Doh, S. Lim, Mode I reflection cracking resistance of strengthened asphalt concretes. Constr. and Build. Mater. 13 (1999) 243-251.

[19] ASTM Standard C1583/C1583M, Standard test method for tensile strength of concrete surfaces and the bond strength or tensile strength of concrete repair and overlay materials by direct tension (pull-off method), ASTM International, West Conshohocken, 2004.

[20] A. Taylor-Firth, I.F. Taylor, A bond tensile strength test for use in assessing the compatibility of Brick / Mortar interfaces. Constr. and Build. Mater. 4 (1990) 58-63.

[21] E.K. Tschegg, K.T. Fendt, C. Manhart, H. Harmuth, Uniaxial and biaxial fracture behaviour of refractory materials. Eng. Fract. Mech. 76 (2009) 2249-2259.

[22] E. de Bilbao, E. Blond, C. Michel, N. Schmitt, T. Cutard, J. Poirier, A new method to determine Young’s modulus of refractory. Interceram, 59 (2010) 34-38.

[23] F. Nazaret, H. Marzagui, T. Cutard, Influence of the mechanical behaviour specificities of damaged refractory castables on the Young's modulus determination. J. of Eur. Ceram. Soc. 26 (2006) 1429-1438.

[24] L. Massard, Etude du fluage de réfractaires électrofondus du système Alumine-Zircone-Silice. PhD thesis, Ecole des Mines de Paris, France, 2005.

[25] O. Bahloul, Evolutions en fonction de la température de propriétés élastiques de bétons réfractaires à base de carbure de silicium, PhD thesis, University of Limoges, France, 2009.

[26] J.C. Almeida, P.B. Lourenço, J.A. Barros, Characterization of brick and brick-mortar interface under uniaxial tension. VII International Seminar on Structural Masonry for Developing Countries, Bello Horizonte, Brazil, 2002.

[27] J.G.M. van Mier, M.R.A. van Vliet, Uniaxial tension test for the determination of fracture parameters of concrete: state of the art. Eng. Fract. Mech. 69 (2002) 235-247.

[28] N. Schmitt, Y. Berthaud, J. Poirier, Tensile behaviour of magnesia carbon refractories. J. of Eur. Ceram. Soc. 20 (2000) 2239-2248.

[29] British Standards Institution BS 6319-4:1984, Testing of resin and polymer/cement compositions for use in construction. Method for measurement of bond strength (slant shear method), BSI. London, 1984.

[30] E.N.B.S. Júlio, F.A.B. Branco, V.D. Silva, J.F. Lourenço, Influence of added concrete compressive strength on adhesion to an existing concrete substrate. Build. and Environ. 41 (2006) 1934-1939.

[31] S. Austin, P. Robins, Y. Pan, Shear bond testing of concrete repairs. Cem. and Concr. Res. 29 (1999) 1067-1076.

[32] D.Raffard, P. Ienny, J.P. Henry, F. Homand, Masonry stone/mortar interface behaviour characterization by optical extensometer. Mech. Res. Commun., 28 (2001) 33-40.

[33] Joint Committee for Guides in Metrology, Evaluation of measurement data - Guide to the expression of uncertainty in measurement. JCGM 100 series. http://www.bipm.org/en/publications/guides/gum.html, 2008 (accessed 3 July 2019).

[34] P.J. Robins, S.A. Austin, A unified failure envelope from the evaluation of concrete repair bond tests. Mag. of Concr. Res. 47 (1995) 57-68.

[35] Z.P. Bažant, Scaling of quasibrittle fracture: asymptotic analysis. Int. J. of Fract. 83 (1997) 19-40.

[36] Mo.Issa, Mh. Issa, M. Islam, A. Chudnovsky, Size effects in concrete fracture: Part I, experimental setup and observations. Int. J. of Fract. 102 (2000) 1-24.